Soy Protein-Based Nanocomposites Reinforced by Supramolecular Nanoplatelets Assembled from Pluronic Polymers/β-Cyclodextrin Pseudopolyrotaxanes

Jin Huang,[1] Ziyan Zhou,[1] Ming Wei,[1] Yun Chen,[2,3] Peter R. Chang[2]

[1]*College of Chemical Engineering, Wuhan University of Technology, Wuhan 430070, China*
[2]*Bioproducts and Bioprocesses National Science Program, Agriculture and Agri-Food Canada, Saskatoon, SK, S7N 0X2, Canada*
[3]*Research Centre for Medical and Structural Biology, School of Basic Medical Science, Wuhan University, Wuhan 430071, China*

Received 30 May 2007; accepted 5 July 2007
DOI 10.1002/app.27075
Published online 20 September 2007 in Wiley InterScience (www.interscience.wiley.com).

ABSTRACT: The self-assembled rigid supramolecular nanoplatelets (SN) from Pluronic polymers with various lengths of polyethylene oxide (PEO) and β-cyclodextrin have reinforced the soy protein isolate (SPI)-based biodegradable plastics in terms of strength and modulus but at the expense of elongation. Meanwhile, the water resistance, which limited the application of the SPI plastics, was also enhanced. The structure and properties of nanocomposites were characterized by X-ray diffraction, differential scanning calorimetry (DSC), scanning electron microscopy (SEM), tensile test, and water uptake test. The low loading of nanoplatelets was able to disperse into SPI matrix homogeneously, which resulted in reinforcement in nanocomposites. With an increase of nanoplatelets loading, the repulsion between nanoplatelets and SPI matrix occurred, accompanying with the formation of rectangle objects, resulted in a decrease of mechanical performance of the nanocomposites. The nanoplatelets with longest free PEO segments produced highest strength with least loss of elongation by virtue of enhanced association with SPI matrix mediated by PEO segments. Meanwhile, the nanoplatelets with moderate length of free PEO segments showed optimal water resistance. Herein, the reinforcing function of a supramolecular nanoplatelet, similar to the structure of layered silicate, was verified. J Appl Polym Sci 107: 409–417, 2008

Key words: nanocomposites; self-assembly; soy protein isolate; mechanical properties; structure–properties relationship

INTRODUCTION

Environmental awareness and the demands of green technology have led to a rapidly increasing interest in the bionanocomposites and/or econanocomposites based on natural polymers, which shows the potential to replace present petrochemical-based materials. It could potentially lead to a strategy for future waste disposal. Recently, such bionanocomposites have been greatly developed by incorporating organic[1,2] and inorganic nano-fillers,[3,4] grafting polymer chains onto nanoparticle surface[5] or self-assembling to form supramolecular nano-phase[6] in the matrix. Soy protein isolate (SPI) can be plasticized by small molecule and hence produce an alternative biodegradable thermoplastics by thermo-moulding.[7] However, the application of SPI-based plastics is limited by water sensitivity, high rigidity, and low rheology[8] as well as a decrease in strength caused by plasticization.[9] As a result, an addition of nano-fillers, the simplest method to prepare nanocomposite, has been attempted to reinforce plasticized SPI-based plastics by virtue of high specific surface area and rigid nature of nano-fillers as well as strong interfacial interactions between nano-fillers and matrix. Recently, the exfoliated layered silicate lamella[3,4,10] have enhanced the strength of SPI-based plastics while the aggregated nano-cluster of spherical nano-SiO_2[11] and the isolated tubular carbon natotube[12] simultaneously reinforced and toughened the materials. Moreover, to further improve the environment-friendliness of the resulting composites, the biodegradable nanoparticles of rod-like cellulose whisker[13] and chitin whisker[14] were incorporated into SPI matrix to produce reinforced plastics with lower water uptake. Meanwhile, the oblatus supramolecular nano-phase, spontaneously

Correspondence to: P. R. Chang (changp@agr.gc.ca).
Contract grant sponsor: Agriculture and Agri-Food Canada; contract grant number: project T.0245.06.
Contract grant sponsor: Canadian Biomass Innovation Network (CBIN); contract grant number: project TID 824.
Contract grant sponsor: National Nature Science Foundation of China; contract grant numbers: 20404014 and 20504010.
Contract grant sponsor: China Postdoctoral Science Foundation; contract grant number: 2004035082.

Journal of Applied Polymer Science, Vol. 107, 409–417 (2008)

aggregated by hydroxylpropyl lignin, in SPI matrix also enhanced the strength.[6,15]

Cyclodextrins (CDs) can thread the polymer chains to produce a rigid and cylindrical supramolecular polyrotaxanes (PRs).[16–18] Especially, there is an increasing interest in the field of materials based on the stretching conformation of polymer in CD channels and rigid PRs rod and its aggregate. The CD-based inclusion was used to create stretching conformation of polymer segments in bulk material and usually removed by water washing or enzymatic degradation after changing the conformation of polymer chain and controlling polymorphic crystalline.[19] The dispersibility between components in the blend was enhanced by the compatiblization of orderly arranged chain regulated by CD strings,[20] in the meanwhile the biodegradability of materials prepared by inclusion and coalescence process was influenced by the degree of microphase separation and crystalline.[21] As expected, the rigid PR rod and its nano-scale aggregate reinforced the epoxy resin, in which the PRs aggregated as dispersed nanodomains tethered by the matrix.[22] At the same time, the wet-spinned cellulose fiber loaded with a moderate content of PRs still resulted in the enhancement of modulus and strength in contrast to pure cellulose fiber. Even though high loading of PRs lowered strength, the blend fibers showed significantly large strain due to the sliding of CD rings along polymer chains.[23] In addition, the PR aggregate became physical cross-linking for the formation of supramolecular hydrogels,[24–27] whose reversible gel-sol transition was sensitive to temperature due to dynamic character of host-guest interaction.[27] Although the reinforcing effect of PR and its nano-aggregate has been discovered, it is not reported so far that the well-defined assemblies based on polymer/CD inclusion are applied for the modification of materials.

Herein, a series of well-defined supramolecular nanoplatelets (SN) has been self-organized from the Pluronic polymers (PEO-*b*-PPO-*b*-PEO) with various polyethylene oxide (PEO) lengths and β-CD.[28] Such SN showed a similar structure to layered silicate lamellae. Meanwhile, the free long PEO segments of the SN are like the grafted chains on the surface of layered silicate lamellae derived from complicated chemical modification, which might improve the associations between nano-filler and matrix to produce the structure of co-continuous phase. In particularly, the rigidity of the SN might contribute to the reinforcement of SPI-based plastics while the free PEO segments with controlled length by varying different Pluronic polymers might affect the association between nanoplatelet and SPI matrix and ultimately affected the mechanical properties. By characterizing the structure and properties of SPI-based nanocomposites filled by various SN, the effects of nanoplatelet structure, especially for the free PEO segments with various lengths, were thereby studied and discussed.

EXPERIMENTAL

Materials

Commercial soy protein isolate (SPI) was purchased from DuPont-Yunmeng Protein Technology Co. (Yunmeng, China). The weight-average molecular weight (M_w) of SPI was determined[6] by multiangle laser light scattering instrument (MALLS, DAWN® DSP, Wyatt Technology Co., Santa Barbara, CA) equipped with a He-Ne laser (λ = 632.8 nm) to be 2.05×10^5. The original moisture content, protein content and amino acid compositions of SPI have been previously reported.[6] All Pluronic polymers (PEO-*b*-PPO-*b*-PEO) were purchased from Aldrich, and three samples containing almost the same propylene oxide (PO) units and various ethylene oxide (EO) units were selected, such as L61 (EO_2-*b*-PO_{30}-*b*-EO_2, $M_n \cong 2000$, 10 wt % of EO content), L64 (EO_{15}-*b*-PO_{30}-*b*-EO_{15}, $M_n \cong 2900$, 40 wt % of EO content), and F68 (EO_{76}-*b*-PO_{30}-*b*-EO_{76}, $M_n \cong 8400$, 80 wt % of EO content). β-Cyclodextrin (β-CD) was supplied by Xi'an Hongchang Pharmacy Co. (Xi'an, China). Glycerol from the Shanghai Chemical Co. (Shanghai, China) was of analytical grade.

Preparation of supramolecular nanoplatelets

β-CD powders were dissolved into distilled water to give a solution with saturation concentration. Subsequently, the aqueous solutions containing a given equivalent weight of Pluronic polymer were added to produce a mixing solution, in which the molar ratio of PO unit vs. β-CD was controlled as ca. 2.0, followed by mechanical stirring for 72 h. The aqueous mixture was observed as white turbidity (the mixture based on F68) or precipitate (the mixtures based on L64 and L61) depending on the length of polyethylene oxide (PEO) segments.

Preparation of nanocomposite sheets

SPI (15 g) was dissolved in 160 mL distilled water at ambient temperature with mechanically stirring to obtain dispersion. Subsequently, an aqueous dispersion containing a desired amount of supramolecular nanoplatelets (SN) was added into SPI dispersion with vigorous stirring for 2 h to produce a homogeneous blend. The resulting solutions were freeze-dried to obtain a series of nanocomposite powders. Herein, the same theoretical number of pseudopolyrotaxane (pseudo-PR) based on the Pluronic polymers with various PEO lengths corresponded to the

TABLE I
Compositions of Nanocomposite Sheets Derived from Supramolecular Nanoplatelets Filled Soy Protein Isolate as Well as SPI-S Sheet

	Supramolecular nanoplatelets per 15 g SPI			
	Pluronic polymer			
Sample code[a]	Category	Content ($\times 10^{-5}$ mol)	Molar ratio of PO vs. β-CD	Weight ratio of powder vs. GL
SL61-0.67	L61	0.67		
SL61-2		2.0		
SL61-4		4.0		
SL61-8		8.0		
SL64-0.67	L64	0.67		
SL64-2		2.0	2 : 1	70 : 30
SL64-4		4.0		
SL64-8		8.0		
SF68-0.67	F68	0.67		
SF68-2		2.0		
SF68-4		4.0		
SF68-8		8.0		
SPI-S		None		

[a] The numbers in the codes represent the theoretical molar number ($\times 10^{-5}$ mol) of PRs assembled from Pluronic polymer/β-CD mixtures based on inclusion ratio of 2 : 1 by PO unit vs. β-CD.

different addition weight, but the difference was very small in contrast to SPI weight.

The freeze-dried nanocomposite powders were mechanical mixed using glycerol as a plasticizer in an intensive mixer (Brabender, Germany), respectively, and the weight ratio of solid powder and glycerol was controlled as 70 : 30. Since the addition content of nanoplatelet based on pseudo-PRs was very small in contrast to the SPI weight, the difference of weight ratio of SPI vs. glycerol might be neglected. Subsequently, 5 g plasticized powders were compression-molded with 769YP-24B hot-press (Tianjin Keqi High Technology Co., Tianjin, China) into a sheet at 140°C under the pressure of 20 MPa for 3 min, and then air-cooled to 50°C before releasing the pressure for demolding. According to the types and the addition contents of Pluronic polymer, the codes for all the molded sheets were summarized in Table I. In addition, the pure SPI sheet, coded as SPI-S, was also prepared according to the above process except for introducing SN.

Characterization of supramolecular nanoplatelets

X-ray diffraction (XRD) patterns of freeze-dried powders were recorded on D/max 2500 X-ray spectrometer (Rigaku Denki, Japan) using Cu Kα (1.54056 Å) radiation (50 kV, 250 mA). All freeze-dried powder samples were mounted on a sample holder and scanned from 3° to 50° in 2θ at a speed of 10° min^{-1}.

Transmission electron microscope (TEM) images were observed using a JEM 100 instrument (JEOL Ltd., Tokyo, Japan) operated at 100 kV as accelerating voltage. The mixing solutions containing assemblies based on Pluronic copolymer and β-CD were spread onto Cu grids coated with carbon films followed by evaporation.

Characterization of nanocomposite sheets

XRD patterns of molded sheets were recorded on D8 Advance diffractometer (Bruker, Karlsruhe, Germany) using Cu Kα (1.54056 Å) radiation (50 kV, 250 mA). The sheet samples were scanned from 3° to 50° in 2θ at a speed of 10° min^{-1}.

DSC analysis was carried out on a DSC-204 instrument (Netzsch, Selb/Bavaria, Germany) under nitrogen atmosphere at a heating or cooling rate of 20°C min^{-1}. The sheets were scanned in the range of −150 to 100°C after a pretreatment (heating from 20 to 100°C and then cooling down to −150°C) of eliminating the thermal history. The resulting thermograms were treated by the accessory software of instrument to get glass transition temperature ($T_{g,mid}$) and heat-capacity increment (ΔC_p) for SPI component as well as melting temperature (T_m) and enthalpy (ΔH_m) for the crystallization of free PEO segments.

Scanning electron microscope (SEM) observation was carried out on a S-570 scanning electron microscope (Hitachi, Ibaraki, Japan). The sheets were frozen in liquid nitrogen and then snapped immediately. The cross-sections were sputtering-coated with gold and then observed and photographed.

The tensile strength (σ_b), elongation at break (ε_b), and Young's modulus (E) of the molded sheets were measured on a CMT6503 universal testing machine (Shenzhen SANS Test Machine Co., Shenzhen,

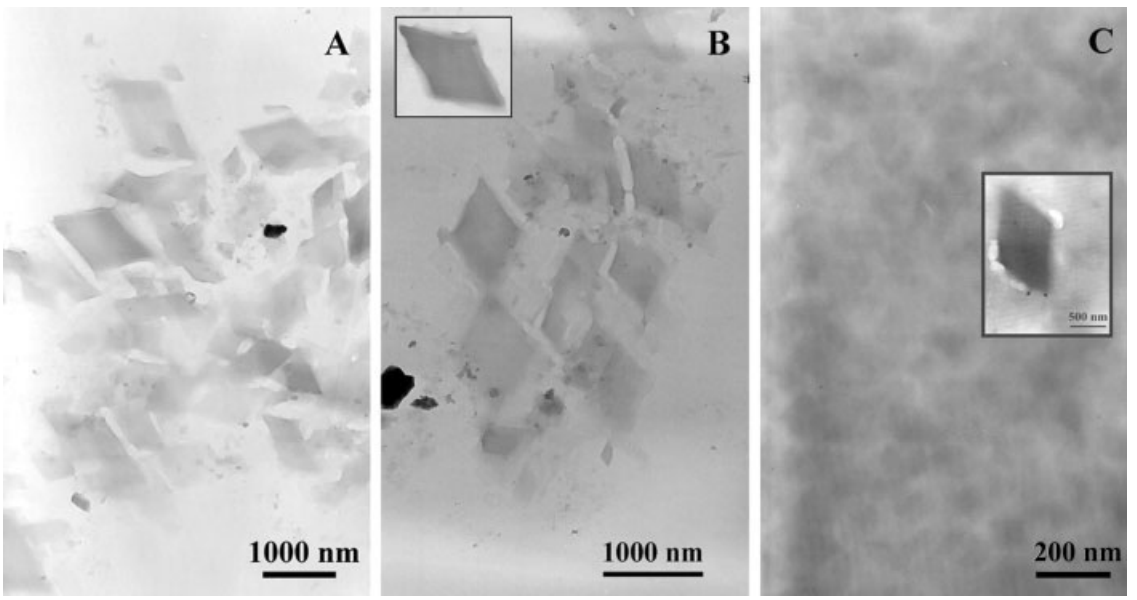

Figure 1 TEM images of self-assembled supramolecular nanoplatelets based on L61/β-CD (A), L64/β-CD (B), and F68/β-CD (C).

China) with a tensile rate of 10 mm min^{-1} according to GB13022-91. The tested samples were cut into the quadrate strips with the width of 10 mm, and the distance between testing marks was 40 mm. The tested strips were kept in a humidity of 35% for 7 days before measurement. An average value of five replicates of each sample was taken.

The water uptake (WU) of the nanocomposite sheets in a controlled relative humidity (RH) was also studied. The specimens used were rectangular sheets with dimensions of 10 mm × 10 mm × ca. 0.5 mm. After weighed as M_0, the specimens were conditioned at room temperature in a desiccator containing saturated $CuSO_4$ aqueous solution (RH of 98%). At specific interval (t), the specimens were taken out and reweighed as M_t. The test is carried out until the weight of sheets uptaking water is invariant, that is, an equilibrium value (M_{00}). The WU content of the specimens was calculated by dividing the gain in weight ($M_t - M_0$) by the initial weight (M_0).[29] An average value of three replicates of each sample was taken.

RESULTS AND DISCUSSION

Structures of supramolecular nanoplatelets

After the β-CDs were mixed with the aqueous solutions of Pluronic polymers, the resulting solution gradually became turbid as the time prolonged and finally produced turbid solution with or without some white precipitate depending on the lengths of PEO segment. Longer PEO chain needed more assembly times while shorter PEO chains easily produced precipitate. Figure 1 shows the TEM images of assemblies in turbid dispersion based on Pluronic polymer and β-CD. For the systems of L61/β-CD and L64/β-CD, the rhombus nanoplatelets with side-length of several hundreds nanometer were observed in Figure 1(A,B). However, as seen in Figure 1(C), the system containing F68 with long PEO chain showed infrequent isolated rhombus nanoplatelet, while the smaller aggregates tended to entangle together by uncovered long PEO chains.

At the same time, XRD patterns of freeze-dried powders from three mixing solutions, as shown in Figure 2, were obviously different from that of pure β-CD, and showed ''channel-type'' crystalline character originated from the orderly stacking of PRs, that is, two predominant diffraction peaks located at 11.7° and 17.6° of 2θ, which was consistent with the previous report.[30] In addition, the crystalline of PEO chains gradually formed as the PEO length increased, shown as two peaks at 18.9° and 23.1° of 2θ assigned to helix crystallization of PEO segments[31] similar to those of free F68. It indicated that most PEO segments were not covered by β-CDs. As a result, the formation and structure of supramolecular nanoplatelet were proposed in Scheme 1, and the β-CDs were drawn along polymer chains mainly in head-to-head and tail-to-tail structures, and occasionally in head-to-tail structure.[32] When the PEO segments were longer, the rhombic nanoplatelet consisted of a sandwich-like structure, that is, the layer of pseudo-PRs' aggregates embedded into two layers of free PEO segments. Such rigid SN showed a similar structure to layered silicate lamellae. Meanwhile, the free long PEO segments of the SN behaved like the grafted chains on the surface of layered silicate lamellae and hence regulated by varying Pluronic polymers.

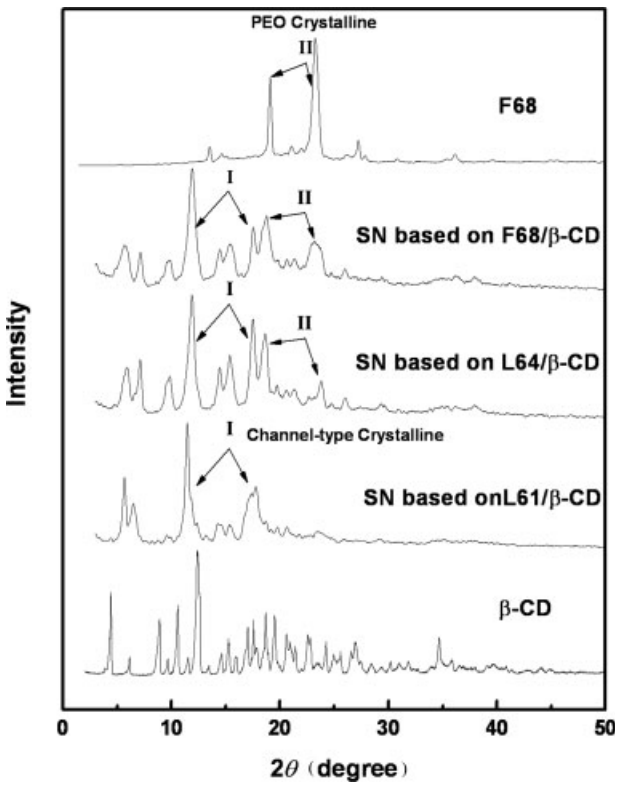

Figure 2 XRD patterns of self-assembled supramolecular nanoplatelets based on L61/β-CD, L64/β-CD, and F68/β-CD as well as F68 and β-CD.

Cross-section of nanocomposites

Figure 3 shows the SEM images of cross-sections of selected nanocomposite sheets and SPI-S sheet. Compared with SPI-S sheet [Fig. 3(A)], the cross-sections of the reinforced nanocomposites with lower nanoplatelet content, such as SL61-0.67 [Fig. 3(B)], SL64-2 [Fig. 3(C)], and SF68-0.67 [Fig. 3(D)], became smooth, indicating that the original ordered structure of SPI matrix was destroyed after introducing nanoplatelet and then resulted in brittle-fraction. With an increase of nanoplatelet content, rectangle crystal-like objects were observed [Fig. 3(E) of SF68-8]. Meanwhile, the other nanocomposites containing high nanoplatelet content showed similar morphology of cross-section in spite of using various nanoplatelets. At this time, the nanocomposite showed distinct rectangle aggregates, which might result in the decrease of mechanical performance.

Effects of supramolecular nanoplatelets on SPI matrix

DSC data of the nanocomposite sheets and F68 are summarized in Table II while the DSC curves of SF68 series and F68 are depicted in Figure 4. Obviously, the addition of nanoplatelets resulted in a decrease of glass transition temperature ($T_{g,mid}$), attributing to the damage of original ordered structures of SPI matrix. With an increase of nanoplatelet content, the nanoplatelets aggregated as great crystal-like objects. At this time, the nanoplatelets and their aggregates were still associated with SPI matrix and hence restricted the motion of SPI chains, resulting in the slight increase of $T_{g,mid}$s for the SL61 and SL64 series. However, too high loading of nanoplatelets led to the repulsion of aggregated objects from SPI matrix, resulting in the decrease of $T_{g,mid}$s in SL61-8 and SL64-8. Different from L61 and L64, long PEO chains in F68 could form crystalline, shown by the melting transition in Figure 4. As regards to SF68-0.67, the nanoplatelet content was lowest while the nanoplatelets homogeneously dispersed into SPI matrix. The melting temperature (T_m) assigned to PEO crystalline was not observed in SF68-0.67. The T_m in SF68-2, SF68-4 and SF68-8 increased slightly with increasing nanoplatelet content while all the T_ms were lower than that of pure F68, indicating that the crystallization of PEO chains was restricted due to the steric hindrance of SPI matrix. On the other hand, the decreasing $T_{g,mid}$ in SF68-2 was attributed to the less restriction of PEO chains to SPI motion after PEO crystallized. Thereafter, the increase of nanoplatelet content led to a slight increase of $T_{g,mid}$ in SF68-4 while highest loading of nanoplatelet induced more severe aggregations and resulted in the lowest $T_{g,mid}$ in SF68-8.

Figure 5 shows XRD patterns of all nanocomposite sheets as well as pure SPI-S sheet. However, it was

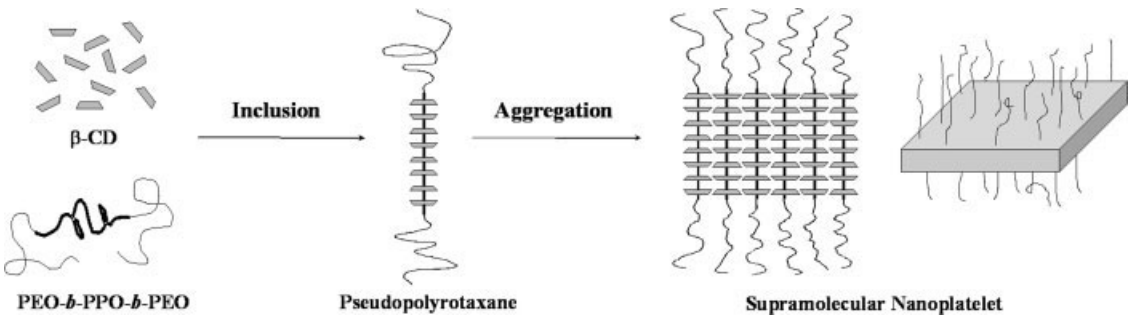

Scheme 1 Formation and proposed structure for self-assembled supramolecular nanoplatelet.

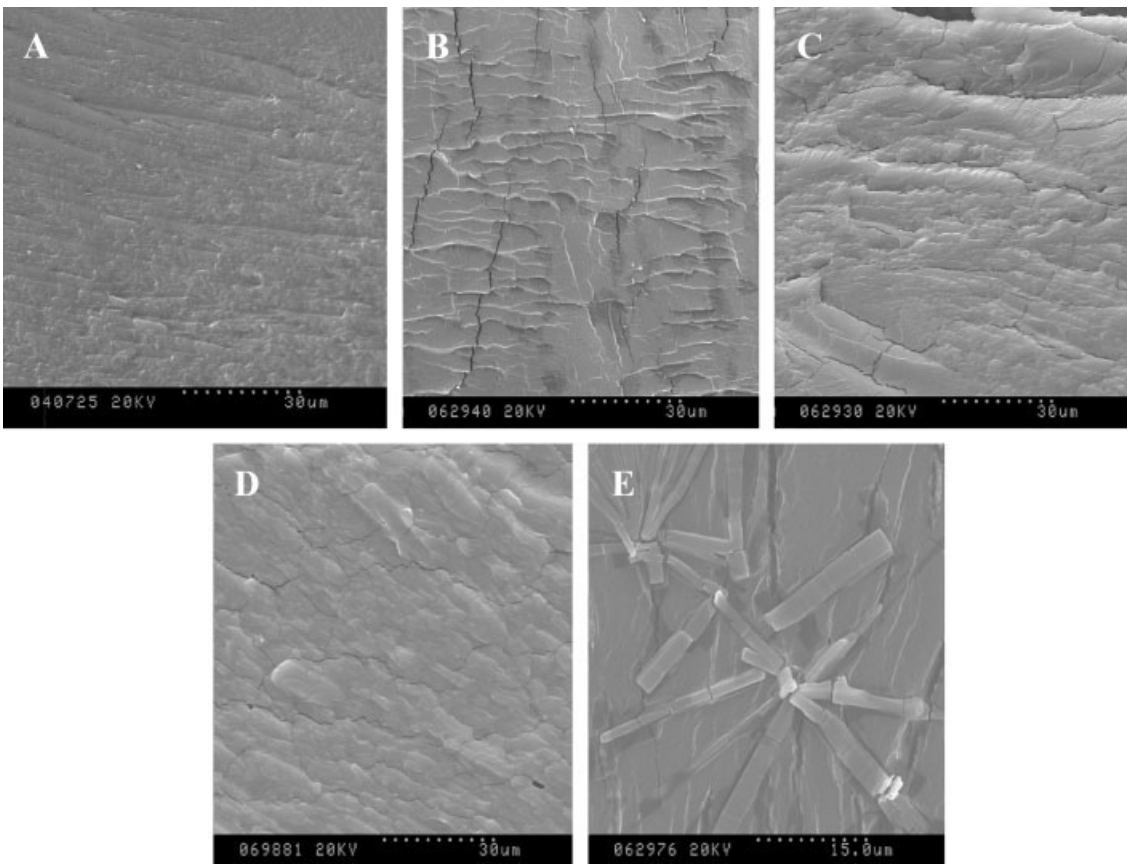

Figure 3 SEM images of cross-section of the selected nanocomposite sheets, such as SL61-0.67 (B), SL64-2 (C), SF68-0.67 (D), and SL64-8 (E), as well as pure SPI-S sheet (A).

unfortunately that the crystalline character of nanoplatelets was not observed in Figure 2 due to the low levels of addition. The XRD pattern of SPI-S suggested that there existed ordered structure, that is, crystalline domains, as evidenced by the two peaks at about 8.8 and 19.0° of 2θ. However, the peak at 8.8° became weaker and even disappeared after introducing nanoplatelets while the peak at 4.7° became visible. It indicated that the addition of nanoplatelets destroyed the original long-range ordered structure in SPI matrix and produced new ordered structure with longer range. The damage of original ordered structure in SPI matrix due to the addition of L61-based nanoplatelet resulted in a decrease of peak intensity at 8.8° until disappearance for SL61-2. However, the distribution of nanoplatelets in SPI matrix in SL61-4 and SL61-8 (both loaded with high levels of nanoplatelets), decreased such damage extent and resulted in the reappearance of peak at 8.8°. For the nanocomposites containing L64-based nanoplatelets, the ordered structure intensity was continually damaged due to the interference of shorter PEO chain, as seen in the gradual drop and the following disappearance of peak at 8.8°. The same interference of PEO chains weakened the peak at 8.8° in SF68-0.67, and this peak eventually disappeared in SF68-2. Thereafter, the crystallization of PEO restricted such damage, and the peak at 8.8° reappeared in SF68-4. However, excess nanoplatelets ultimately destroyed original ordered structure of SPI matrix in SF68-8, as evidenced by the absence of peak at 8.8° once more.

TABLE II
DSC Data of the Sheets Based on SPI/SN Nanocomposites and SPI as Well as SPI Powder and F68

Sample	$T_{g,mid}$ (°C)	ΔC_p (J g^{-1} K^{-1})	T_m (°C)	ΔH_m (J g^{-1})
SL61-0.67	−46.2	0.603	–	–
SL61-2	−45.1	0.554	–	–
SL61-4	−44.1	0.701	–	–
SL61-8	−46.6	0.656	–	–
SL64-0.67	−46.0	0.643	–	–
SL64-2	−43.4	0.665	–	–
SL64-4	−44.9	0.646	–	–
SL64-8	−46.1	0.638	–	–
SF68-0.67	−47.3	0.662	–	–
SF68-2	−48.8	0.625	47.7	0.432
SF68-4	−47.5	0.600	48.1	1.005
SF68-8	−50.4	0.607	48.3	1.979
SPI-S	−41.3	0.642	–	–
F68	–	–	56.6	119.5

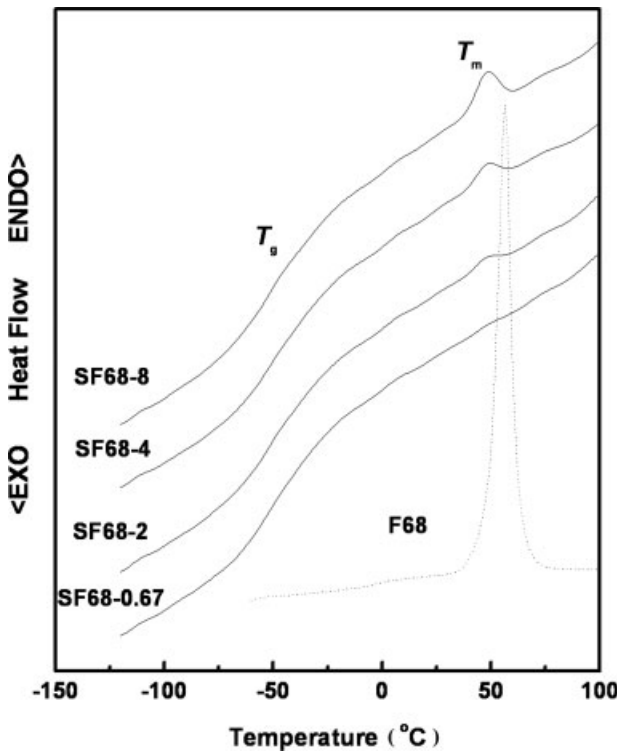

Figure 4 DSC curves of SF68 sheets containing various content of nanoplatelets based on F68/β-CD as well as the reference of F68.

Mechanical properties of nanocomposites

The effects of pseudo-PR (the building unit of nanoplatelet) content on the mechanical properties of the resulting nanocomposite sheets are depicted in Figure 6. Some nanocomposite sheets containing moderate content of assembled nanoplatelets with various lengths of free PEO chains on the surface showed an enhanced strength with the expense of elongation. For the nanocomposite filled by L61-based nanoplatelets, SL61-0.67 containing least nanoplatelets exhibited the maximum tensile strength (σ_b) of 8.78 MPa as well as an increase of the Young's modulus (E) up to 192.5 MPa. Thereafter, with an increase of pseudo-PR content, the strength decreased while the modulus increased and reached the maximum at SL61-4. However, SL64-0.67 containing least L64-based nanoplatelet showed a sharp decrease of strength and modulus, and then reached maximum strength (7.86 MPa) and modulus for SL64-2. Subsequently, increasing the pseudo-PR content resulted in the gradual decrease of strength and modulus. The enhancement of strength attributed to the uniform distribution of nanoplatelets in SPI matrix when the pseudo-PR content was low. Meanwhile, the formation of great-scale aggregates weakened the reinforcing function and gave decreased strength with an increase of pseudo-PR content. It was regretful that that both systems showed a gradual decrease of elongation at break (ε_b) with an increase of pseudo-PR content. The nanoplatelets with uncovered long PEO chains showed optimal reinforcing effects with lowest expense of elongation for SPI-based plastics. The maximum strength reached 9.19 MPa for SF68-0.67 while SF68-2 could keep elongation of 102.5% at break. Similarly, high loading of nanoplatelet resulted in decrease of strength, elongation, and modulus.

Water resistance after introducing nanoplatelets

The diffusion of water is strongly influenced by microstructure of nanocomposites, which affects gas, water, and solute permeability.[29] The water uptake

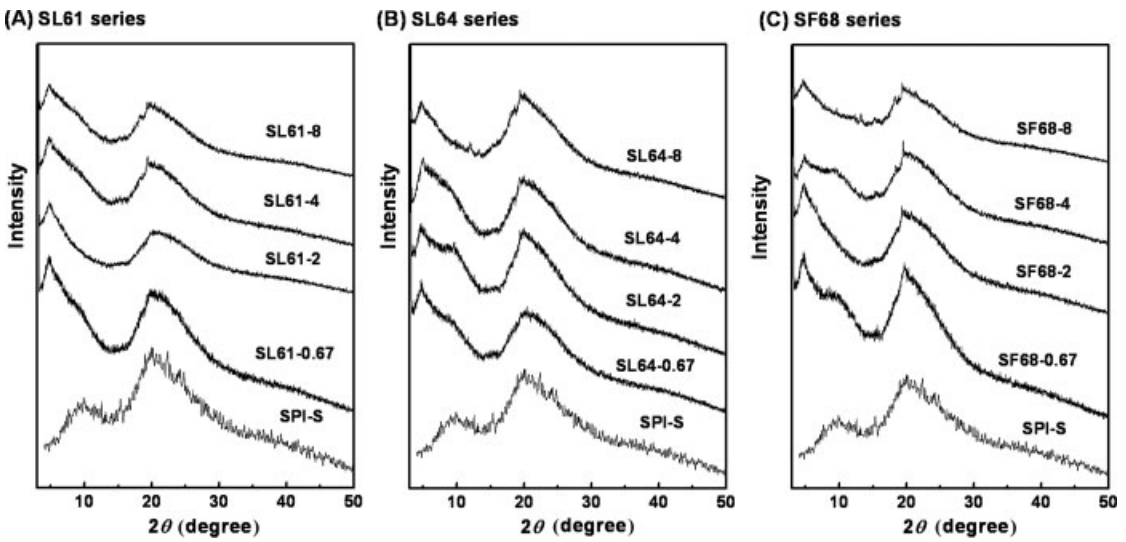

Figure 5 XRD patterns of SPI-based sheets modified by assembled nanoplatelets based on L61/β-CD (A), L64/β-CD (B), and F68/β-CD (C) as well as SPI-S sheet.

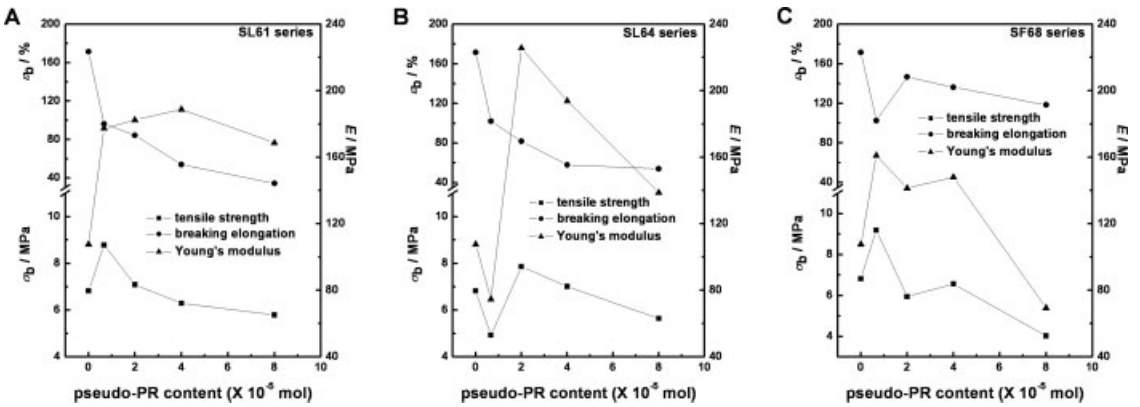

Figure 6 Mechanical properties of SPI-based sheets modified by assembled nanoplatelets based on L61/β-CD (A), L64/β-CD (B), and F68/β-CD (C).

up to equilibrium of nanocomposite and SPI-S sheet under relative humidity (RH) of 98% is plotted as a function of time (t) in Figure 7. Two distinct zones were observed as Zone I ($t < 150$ h) for the rapid increase of water uptake and Zone II ($t > 150$ h) for reaching the equilibrium, respectively. Except for SL61-8 with highest loading of nanoplatelet, all the other testing nanocomposites showed lower water uptake of about 30% than SPI-S sheet. For the SL64 and SL68 nanocomposites, the water uptake was almost independent of nanoplatelet content added. When the length of PEO chain was moderate, the SL64 nanocomposites had lowest water uptake of about 26%. Meanwhile, the increasing water uptake of SL61-8 attributed to more sever aggregations induced by the repulsion of excess nanoplatelets from SPI matrix as well as the absence of associating SPI matrix mediated by PEO chain.

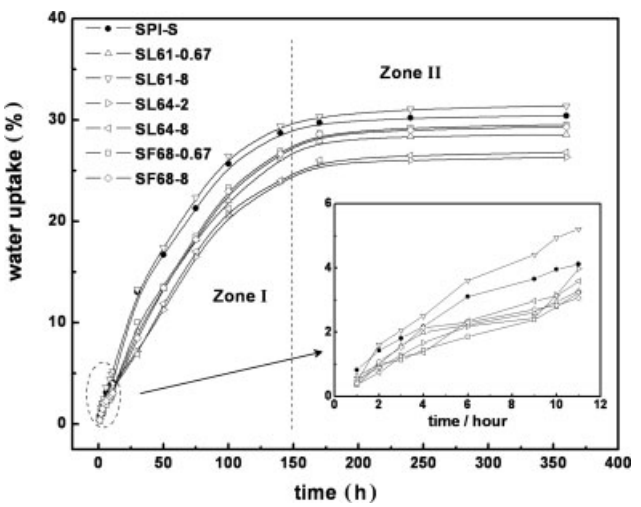

Figure 7 Water uptake of the nanocomposite sheets filled by various nanoplatelets and SPI-S sheet under relative humidity of 98%.

CONCLUSIONS

A series of rigid supramolecular nanoplateles with adjustable structure has been assembled from Pluronic polymers and β-cyclodextrin, and then was used to reinforce soy protein-based plastics as well as to enhance water resistance. A small amount of nanoplatelets was able to disperse uniformly into SPI matrix to produce optimal strength and modulus. With an increase of nanoplatelet content, the repulsion between added nanoplatelets and SPI matrix occurred accompanying with the formation of rectangle objects, resulting in the decrease of mechanical performance. The nanoplatelets with longest free PEO segments produced highest strength with less expense of elongation by virtue of enhanced association with SPI matrix mediated by PEO chains. Meanwhile, the nanoplatelets with moderate length of free PEO segments showed optimal water resistance. Thereupon, a strategy has been put forward to regulate properties of nanocomposites by controlling the structures of added supramolecular nanoparticles based on the combination character of self-assembly.

References

1. Angellier, H.; Molina-Boisseay, S.; Dole, P.; Dufresne, A. Biomacromolecules 2006, 7, 531.
2. Sriupayo, J.; Supaphol, P.; Blackwell, J.; Rujiravanit, R. Carbohydr Polym 2005, 62, 130.
3. Chen, P.; Zhang, L. Biomacromolecules 2006, 7, 1700.
4. Yu, L.; Dean, K.; Li, L. Prog Polym Sci 2006, 31, 576.
5. Thielemans, W.; Belgacem, M. N.; Dufresne, A. Langmuir 2006, 22, 4804.
6. Wei, M.; Fan, L.; Huang, J.; Chen, Y. Macromol Mater Eng 2006, 291, 524.
7. Sue, H. J.; Wang, S.; Jane, J. Polymer 1997, 38, 5035.
8. Kumar, R.; Choudhary, V.; Mishra, S.; Varma, I. K.; Mattiason, B. Ind Crop Prod 2002, 16, 155.
9. Wang, S.; Sue, H. J.; Jane, J. J Macromol Sci A Pure Appl Chem 1996, 33, 557.

10. Yu, J.; Cui, G.; Wei, M.; Huang, J. J Appl Polym Sci 2007, 104, 3367.
11. Ai, F.; Zheng, H.; Wei, M.; Huang, J. J Appl Polym Sci 2007, 105, 1597.
12. Zheng, H.; Ai, F.; Wei, M.; Huang, J.; Chang, P. R. Macromol Mater Eng 2007, 292, 780.
13. Wang, Y.; Cao, X.; Zhang, L. Macromol Biosci 2006, 6, 524.
14. Lu, Y.; Weng, L.; Zhang, L. Biomacromolecules 2004, 5, 1046.
15. Chen, P.; Zhang, L.; Peng, S.; Liao, B. J Appl Polym Sci 2006, 101, 334.
16. Wenz, G.; Han, B.-H.; Muller, A. Chem Rev 2006, 106, 782.
17. Huang, F. H.; Gibson, H. W. Prog Polym Sci 2005, 30, 982.
18. Harada, A. Adv Polym Sci 1997, 133, 141.
19. Rusa, C. C.; Wei, M.; Bullions, T. A.; Rusa, M.; Gomez, M. A.; Porbeni, F. E.; Wang, X.; Shin, I. D.; Balik, C. M.; White, J. L.; Tonelli, A. E. Cryst Growth Design 2004, 4, 1431.
20. Wei, M.; Tonelli, A. E. Macromolecules 2001, 34, 4061.
21. Shuai, X.; Wei, M.; Porbeni, F. E.; Bullions, T. A.; Tonelli, A. E. Biomacromolecules 2002, 3, 201.
22. Wang, X.-S.; Kim, H.-K.; Fujita, Y.; Sudo, A.; Nishida, H.; Endo, T. Macromolecules 2006, 39, 1046.
23. Araki, J.; Kataoka, T.; Katsuyama, N.; Teramoto, A.; Ito, K.; Abe, K. Polymer, 2006, 47, 8241.
24. Li, J.; Li, X.; Zhou, Z.; Ni, X.; Leong, K. Macromolecules 2001, 34, 7236.
25. Huh, K. M.; Ooya, T.; Lee, W. K.; Sasaki, S.; Kwon, I. C.; Jeong, S. Y.; Yui, N. Macromolecules 2001, 34, 8657.
26. Sabadini, E.; Cosgrove, T. Langmuir 2003, 19, 9680.
27. He, L. H.; Huang, J.; Chen, Y. M.; Xu, X. J.; Liu, L. P. Macromolecules 2005, 38, 3845.
28. Huang, J. Block-Copolymer Assembly Induced by Host-Guest Interaction; Postdoctoral Research Report, Institute of Chemistry, Chinese Academy of Sciences, 2005.
29. Anglès, M. N.; Dufresne, A. Macromolecules 2000, 33, 8344.
30. Harada, A.; Okada, M.; Li, J.; Kamachi, M. Macromolecules 1995, 28, 8406.
31. Tadokoro, H.; Chatani, Y.; Yoshihara, T.; Tahara, S.; Murahashi, S. Macromol Chem 1964, 73, 109.
32. Miyake, K.; Yasuda, S.; Harada, A.; Sumaoka, J.; Komiyama, M.; Shigekawa, H. J Am Chem Soc 2003, 125, 5080.